


RESEARCH ARTICLE | MAY 20 2025

Modal gain tailoring by flat stamping of thin colloidal films ✓Ruslan Azizov ✉ ; Jinlong Zhu ; Pavel Talianov ; Furkan Isik ; Hilmi Volkan Demir ; Sergey Makarov ✉ *Appl. Phys. Lett.* 126, 203301 (2025)<https://doi.org/10.1063/5.0266347>**Articles You May Be Interested In**

Direct laser writing of resonant periodic nanostructures in thin light-emitting films of CdSe/CdZnS core/shell nanoplatelets

Appl. Phys. Lett. (November 2022)

Plasmonic gain in long-range surface plasmon polariton waveguides bounded symmetrically by dye-doped polymer

Appl. Phys. Lett. (September 2015)

Synthesis and Characterization of Nanocrystalline CdZnS Thin Films

AIP Conf. Proc. (July 2011)**Applied Physics Letters****Special Topics Open
for Submissions**[Learn More](#)

Modal gain tailoring by flat stamping of thin colloidal films

Cite as: Appl. Phys. Lett. **126**, 203301 (2025); doi: [10.1063/5.0266347](https://doi.org/10.1063/5.0266347)

Submitted: 18 February 2025 · Accepted: 2 May 2025 ·

Published Online: 20 May 2025



View Online



Export Citation



CrossMark

Ruslan Azizov,^{1,2,a)} Jinlong Zhu,¹ Pavel Talianov,¹ Furkan Isik,³ Hilmi Volkan Demir,^{3,4} and Sergey Makarov^{1,2,a)}

AFFILIATIONS

¹Qingdao Innovation and Development Center, Harbin Engineering University, 266000 Qingdao, China

²School of Physics and Engineering, ITMO University, 197101 St Petersburg, Russia

³Department of Electrical and Electronics Engineering and Department of Physics, UNAM—Institute of Materials Science and Nanotechnology, Bilkent University, Ankara 06800, Turkey

⁴Luminous! Center of Excellence for Semiconductor Lighting and Displays, School of Electrical and Electronic Engineering, School of Physical and Mathematical Sciences, School of Materials Science and Engineering, Nanyang Technological University, Nanyang Avenue, Singapore 639798, Singapore

^{a)}Authors to whom correspondence should be addressed: ruslan.azizov@metalab.ifmo.ru and s.makarov@metalab.ifmo.ru

ABSTRACT

Post-synthetic tailoring and improvement of the light-emitting material properties is an important direction for optimization of solution processible LEDs and recently emerged laser diodes based on nanocrystals. In this study, we demonstrate modal gain engineering by flat stamping light-emitting films of core/alloyed shell CdSe/CdZnS nanoplatelets. This film modification approach affects the volume density occupation (D) of the emitters in the film and allows for control of the layer thickness while keeping surface roughness low and uniformity high. The achieved level of control of the mode confinement factor (Γ) and optical gain is promising for better integration with resonators and multilayered structures. Careful accounting of such parameters makes it possible to achieve higher D values and increase the modal gain up to ~ 2.39 times in comparison with standard spin-coating films. The modal gain enhancement and the Γ factor control allow us to maximize the optical gain in light-emitting devices and facilitate low-threshold lasing.

Published under an exclusive license by AIP Publishing. <https://doi.org/10.1063/5.0266347>

The quality of the light-emitting layer made of solution-processable materials is a key parameter in modern light-emitting diodes (LEDs) and lasers.¹ Colloidal semiconductors' main advantage over their epitaxially grown counterparts is the availability of various low-cost deposition techniques,^{2,3} which can be used if high optical gain values and other key parameters can be achieved.

From the material point of view, the realization of lasers requires several conditions to be met. First, the buildup of optical gain (population inversion) processes should be protected from the impact of fast non-radiative Auger recombination, which requires additional material engineering.⁴ Second, integration with the optical cavity demands the creation of an active medium with precisely calculated thickness, preserving the quality and emissive characteristics of the layer while supporting the desired optical mode. Finally, the device design should minimize optical losses while maintaining the electromagnetic field effectively.⁵ Material engineering directly affects the value of material gain (g_{mat}) and, thus, contributes to the modal gain coefficient (g_{mod})

and amplified spontaneous emission (ASE) threshold. The modification of intrinsic properties implies the complex challenge for the control of radiative and non-radiative energy recombination mechanisms complicated by extrinsic factors, which often leads to a trade-off between lowering the ASE threshold and increasing the maximum value of g_{mod} .

In turn, core-shell nanocrystals in the form of nanoplatelets (NPLs) made of II-VI semiconductors are one of the most promising families of materials for the creation of both optically and electrically pumped solution-processable lasers.^{6–10} However, optimization of the modal gain coefficient for the deposited thin films is still a big challenge, which prevents the development of commercialized laser diodes.¹¹ Although changing the NPL shell type from CdSe/CdSeTe core/alloyed crown¹² to CdSe/CdSeTe/CdS core/multicrown¹³ allowed us to reduce the ASE threshold from 26 to 4 $\mu\text{J}/\text{cm}^2$, it also reduced g_{mod} values by 0.56 times at the same emission wavelength. When comparing reported studies with CdSe/CdS/CdZnS, changing the

design from core/crown/shell¹⁴ to core/shell/shell¹⁵ resulted in an increase in g_{mod} by only 4.5% while reducing the ASE threshold from 31 to 17.3 $\mu\text{J}/\text{cm}^2$. In light of the above, to better preserve charge carrier recombination energy with a minimum loss to Auger processes, NPLs should have a shell with a continuously graded composition.^{4,16} In this regard, specially engineered core/alloyed shell CdSe/CdZnS nanoplatelets (NPLs), also known as colloidal quantum wells (CQWs), demonstrate a large absorption cross section and a long biexciton radiative lifetime, as well as strong Auger suppression.¹⁷

Also, the resulting optical gain depends on the layer thickness and the efficiency of active layer integration with the optical cavity, which could be estimated via the mode confinement factor (Γ). For the NPLs, the refractive index contrast at the boundary of the active layer and the substrate contributes to an increase in Γ from 1% on bare fused silica to 19.5% on 55 nm thick TiO_2 with a light-emitting layer thickness of 42 nm.¹⁸ At the same time, g_{mod} growth by 1.86 times was noted with the increase in the NPL layer thickness from 21 to 28 nm. While in other work, an increase in the active layer thickness from 100 to 250 nm led to a g_{mod} decrease by 2.3 times due to a reduction of the optical pumping efficiency.¹⁹

On the contrary, there is a large variety of NPL deposition methods, such as drop-casting,²⁰ spin-coating,²¹ dip-coating,²² and slot-dye,³ and each method has different resulting homogeneity of film thickness, smoothness quality, and NPL package volume density, which eventually affect g_{mod} . For example, the atomic-scale distance variation between NPLs is a key factor in the transfer of electrons by the hopping process.^{23,24} In this regard, the direct way to increase g_{mod} is to improve the volume density occupation of the emitters in the film (D). This effect was demonstrated when the transition from drop-casting²⁰ to spin-coating (SC)²¹ resulted in a 1.15-fold gain enhancement in CdSe NPLs. In turn, SC approach usually faced a problem of so-called coffee-ring formation, which also affected D and the final quality of the film, resulting in g_{mod} reduction. Therefore, a cost-effective and simple approach is needed for better control of NPL thin film parameters and make them more suitable for lasing applications.²⁵

In this work, we apply a flat stamping method to demonstrate the NPL layer modal gain engineering by modifying the thickness, roughness, and D values of the film to overcome the problems after the deposition. By optimizing the applied pressure on the stamp, we achieve a shorter interparticle distance, which improves D values of the NPL layer. As a result, the described approach lets us increase g_{mod} up to 2.39 times for core/alloyed shell CdSe/CdZnS nanoplatelet layers and can be applied as an additional step to all the solution-processable nanomaterials where the spin-coating method is used for deposition. In general, the application of flat stamping gives an opportunity for better light-emitting layer integration with resonators and multilayered systems by controlling the Γ factor and affecting optical gain efficiency in an active medium.

In our experiments, we used the SC method to create samples with different thicknesses from NPL solution in hexane with a concentration of 50 mg/ml (samples names: SC1, SC2, and SC3) and 25.6 mg/ml (SC4) by deposition on a glass substrate. At a rotation speed of 700 rpm for SC1 and SC4, and 1000 rpm for SC2 and SC3, 60 μl of solution was applied and spinned for a minute. Additionally, the samples prepared by the SC method as well as by the layer-by-layer deposition technique from the NPL solution with a concentration of 25.6 and 128.5 mg/ml were investigated (see the [supplementary](#)

[material](#)). Atomic force microscopy (AFM, HORIBA SmartSPM - 1000) measurements yielded average thickness values around 204.3 nm (SC1), 205.1 nm (SC2), 161.6 nm (SC3), and 69.96 nm (SC4) (the roughness data are given in Table S1). The thickness values of the samples were employed in our ellipsometry measurements with a commercial ellipsometer Accurion EP4.

To investigate the influence of the material volume density on optical gain characteristics, the spin-coated NPL films were modified by flat stamping as schematically shown in [Fig. 1\(a\)](#). In the stamping process, standard glass slides ($1 \times 1 \text{ cm}^2$) were used as a stamp. The size of the stamps, smaller than the samples ($1 \times 1.5 \text{ cm}^2$), made it possible to directly compare the optical characteristics of the exactly same NPL film before and after the stamping [[Figs. 1\(b\)](#) and [1\(c\)](#)].

The stamping regime consists of applying the pressure on the stamp for 5 min: 1500 kg/cm² on SC1 and SC3, and 1000 kg/cm² on SC2 and SC4. A decrease in thickness on average to 137.4 nm (SC1S), 133.4 nm (SC2S), 143.3 nm (SC3S), and 44.3 nm (SC4S) were observed. The modal gain characteristics of the obtained samples were measured using the variable stripe length (VSL) technique (see details in the [supplementary material](#)).²⁶ The features in the intensity growth of the ASE peak of the samples were investigated at four fluences: 78.4, 209, 418, and 784 $\mu\text{J}/\text{cm}^2$ (Table S1). Such a range was chosen because the NPL gain growth saturation effect is weak when we compare it to the classical quantum dots (QD). This can be explained by the higher surface area, which led to the multiexcitonic properties dominating that higher gain saturation threshold in one order from the onset of gain.²⁷ The effect of stamping on the g_{mod} values of sample SC3 is illustrated in [Figs. 1\(b\)](#) and [1\(c\)](#), as the representative sample.

To interpret the measured data, the small signal gain model was implemented,²⁶

$$I = \frac{A}{g_{\text{net}}} (e^{g_{\text{net}} \times L} - 1), \quad (1)$$

where I is the ASE peak intensity, A is the optical growth factor, L is the stripe length of the excitation beam, and g_{net} is the obtained net modal gain. The small signal gain model assumes linearity of intensity growth at low fluences, and the g_{net} values' range coincides with the values obtained from similar NPLs.^{13,15,18} The net modal gain can be expressed as

$$g_{\text{net}} = \Gamma \times D \times g_{\text{mat}} - \alpha, \quad (2)$$

where g_{mat} is the material gain, which is related to the material light-emission properties.¹⁸ The loss coefficient α contains contributions from light absorption and scattering during propagation through the layer. Here, Γ is a "mode confinement" factor defined by the degree of optical mode confinement within the gain medium,

$$\Gamma = \int_{\text{NPLs}} \frac{1}{2} \text{Re}\{E \times H^*\} \hat{z} dx dy / \int_{-\infty}^{\infty} \frac{1}{2} \text{Re}\{E \times H^*\} \hat{z} dx dy, \quad (3)$$

where E and H are the electric and magnetic fields at fixed z , respectively. The integral in the numerator is evaluated across the optically active portion of the waveguide, the NPL layers.¹⁸

Therefore, the device design parameters, such as thickness and refractive indexes, affect the modal gain value through Γ , but even in

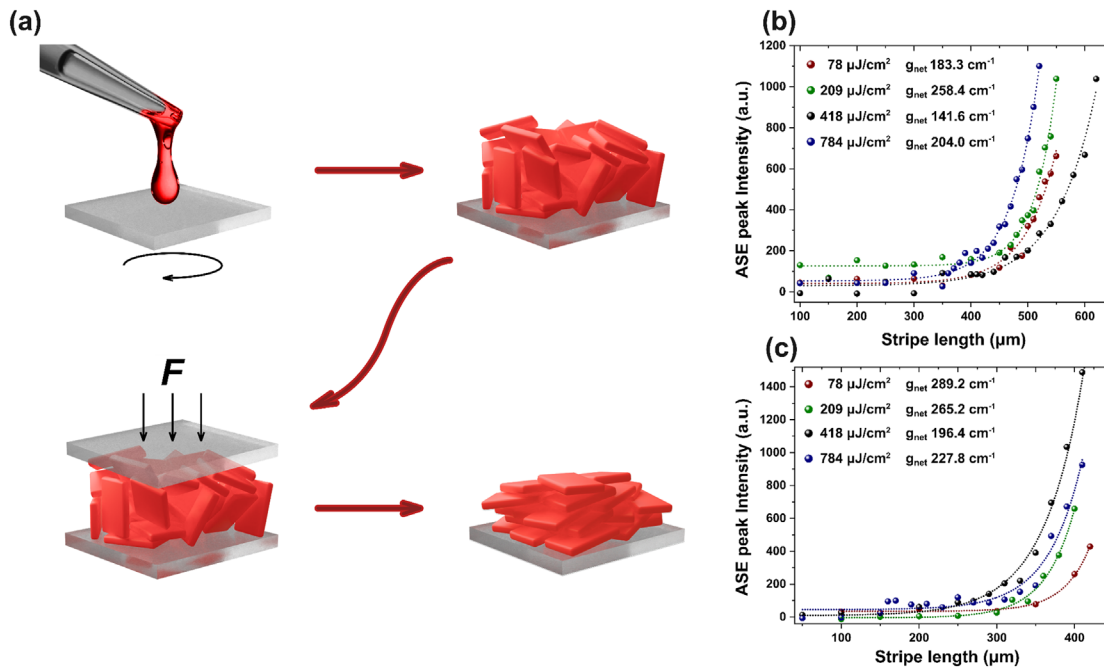


FIG. 1. (a) Sample preparation scheme. Net modal gain measurements result from initial SC3 (b) and stamped SC3 (c) part of the sample at different fluences made by the variable stripe length method.

well-designed optical gain electroluminescent devices, the mode confinement can reach values $\Gamma = 0.3$ – 0.4 only.¹

We evaluated the effect of the flat stamping on the physical properties of spin-coated NPL films, thereby on the mode confinement factor Γ . The stamping process improves the surface quality (root mean square, RMS) of sample SC1S up to 3.03 nm [Figs. 2(a) and 2(d)] and for sample SC2S up to 4.2 nm, while for the sample SC3S, it slightly decreased to 4.23 nm, and to 5.11 nm for sample SC4S. Such differences are due to the carefulness of the stamping process and indicate the high initial quality of the films.

AFM measurements of samples SC1 and SC1S indicate that the surface structure is preserved during the stamping process. However, it resulted in changes in the light-emitting properties of the layer. To image the impact of stamping on the NPL films, we used SEM with an InLens (Zeiss Crossbeam 350) secondary electron detector. The SEM image in Fig. 2(b) shows that the sample on a glass substrate after stamping (right part) has a brighter shade. The depth of the material layer from which we collect the signal at such a regime is about a hundred of nanometers. The increase in the material volume density after stamping results in a rise of the signal intensity from the modified part (Fig. S3). The measured ASE threshold $17.8 \mu\text{J}/\text{cm}^2$ [Fig. 2(e)] is comparable with the similar II-VI NPLs reported previously.^{12,15,28,29} The PL peak position was at $\lambda = 641 \text{ nm}$ while the ASE peak is redshifted in 15 nm for the sample SC2 [Figs. 2(c) and 2(f)].

On the n and k curves of the NPLs, there are two characteristic excitonic peaks referring to light and heavy holes.³⁰ The n , k values of the initial sample were measured by visualizing an ellipsometer in a range of wavelengths 400–800 nm (Fig. S1). Despite the lack of material density control in SC technique, the n , k values (see additional

materials) agree with the results in the previous works for similar materials.³¹

To calculate the Γ factor by the software Comsol Multiphysics, the refractive index at a wavelength corresponding to the samples' ASE band peak, as well as the NPL layer thickness of each sample, were taken (Fig. S5). The Γ parameter of the initial films was at the level of 0.93 for SC1, 0.93 for SC2, and 0.86 for SC3, which is mostly due to the difference in the sample thickness. The waveguiding effect determines the layer thickness limit under which the Γ factor drops dramatically. The SC4 sample, with its low thickness, is characterized by the significant influence of the waveguide process in the substrate on the light-emitting properties of the sample and calculated Γ values 0.1 far from the effective one [Fig. S5(b)].

Parameter Γ decreases after the stamping process due to the reduction of the samples' thickness on average, to the level of 0.82 for SC1S, 0.77 for SC2S, and 0.85 for SC3. The influence of Γ and NPL layer quality coincides with the results obtained when measuring the g_{net} of the samples. The surface quality improvement decreases the losses during the waveguiding component of α , supporting an increase in gain (Table S2).

Parameter Γ mostly depends on the refractive index (n) contrast and thickness of the light-emitting layer, while g_{mod} could be estimated by the stimulated emission cross section (σ_e) and density of the population inversion ($N_{\text{pop.inv.}}$),

$$g_{\text{net}} = \Gamma \times \sigma_e \times N_{\text{pop.inv.}} - \alpha = \Gamma \times \sigma_e \times n_t \times \frac{\frac{F_p}{F_s}}{1 - \frac{F_p}{F_s}} - \alpha, \quad (4)$$

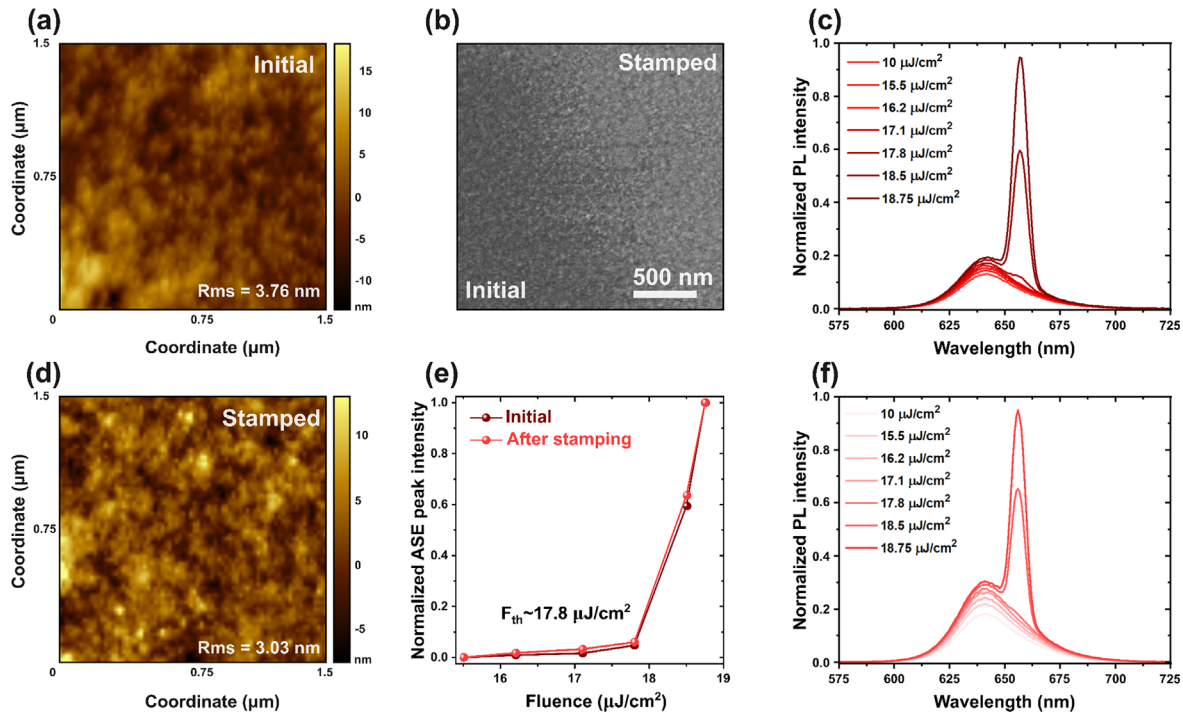


FIG. 2. AFM images of sample SC1 before (a) and SC1S after (d) stamping by $1500 \text{ kg}/\text{cm}^2$. (b) SEM image of a sample border between SC1 (left) and SC1S (right). ASE spectral behavior of sample SC2 (c) and SC2S (f). (e) ASE intensity dependences on incident pumping fluence for the sample SC2 before and SC2S after stamping by pressure $1000 \text{ kg}/\text{cm}^2$.

where n_t is the density of active centers, F_p is the pump fluence, and F_s is the single-exciton saturation pump fluence level.⁶

By using Eq. (4), it is possible to assess the influence of the stamping effect on g_{mod} of the NPL layer. Increasing the material volume density and, as a consequence, the n_t value (equal to D), brings the g_{mod} closer to g_{mat} —the value depending only on the intrinsic property of the NPLs.

With the decrease in the thickness of the light-emitting layer, the Γ values also decrease dramatically, critically affecting optical gain properties. To estimate such an effect on parameter Γ , simulation in the Comsol Multiphysics was performed with a different refractive index [Fig. 3(a)]. The high refractive index of the light-emitting material allows us to achieve high Γ values even from a layer tens of nanometers thick.

The key parameter affecting g_{mod} is the density of active centers n_t and α , which could be estimated by fitting measured values of g_{net} at different fluences [Fig. 3(b)]. For all the samples, parameter α was fitted separately and found to correlate with surface roughness (see Table S2).^{15,18} The saturation pump fluence level F_s for all the samples was affected by several conditions: NPLs are the same between all the samples; no additional layers are added to affect the Γ , but the material volume density and layer quality affect stimulated emission propagation through the NPL layer. During the fitting, stimulated emission cross section σ_e value of $4.32 \times 10^{-15} \text{ cm}^2$ was taken from the article by Foroutan-Barenji *et al.* due to the fact that this is a characteristic value of the CdSe/CdZnS NPLs itself.¹⁸

The net modal gain data analysis [Fig. 3(c)] shows that the highest g_{mod} value of 476.2 cm^{-1} among the initial samples has SC3 with $n_t = 111.2 \times 10^{15} \text{ cm}^{-3}$. It should be noted that samples SC2 and SC3 applied at 1000 rpm had different thicknesses after deposition. Sample SC2 with a greater thickness was characterized by lower n_t values $75.2 \times 10^{15} \text{ cm}^{-3}$ and caused its lower g_{mod} values 321.5 cm^{-1} compared to SC3. Sample SC1, with almost the same thickness as SC2, also had low n_t and g_{mod} values of 268.1 cm^{-1} . As an additional fact, a smaller layer thickness allows more uniform pump distribution. This effect determines a higher g_{mod} for thin samples.¹⁸

After the stamping process, the g_{mod} values of all samples increased. The most noticeable increase was observed in samples SC1S and SC3S stamped at a higher pressure— $1500 \text{ kg}/\text{cm}^2$, which made it possible to increase D to the greatest extent. The highest improvement in the g_{mod} values up to 639.8 cm^{-1} is noted for sample SC1S. This suggests that, initially, the sample had the lowest material volume density, which determined $n_t = 62.6 \times 10^{15} \text{ cm}^{-3}$ of the layer. Taking this into account, spin-coating at 700 rpm made it possible to obtain the highest g_{mod} values after stamping due to the largest initial amount of material on the substrate, which made it possible to achieve the maximum density of active centers $n_t = 151 \times 10^{15} \text{ cm}^{-3}$. By comparing the obtained maximum value with $n_t = 459 \times 10^{15} \text{ cm}^{-3}$ inherent to the calculated $g_{mat} = 1850 \text{ cm}^{-1}$ at $1000 \mu\text{J}/\text{cm}^2$ of the NPLs,¹⁸ the ratio of the gain and n_t values is preserved and justifies the obtained g_{mod} values.

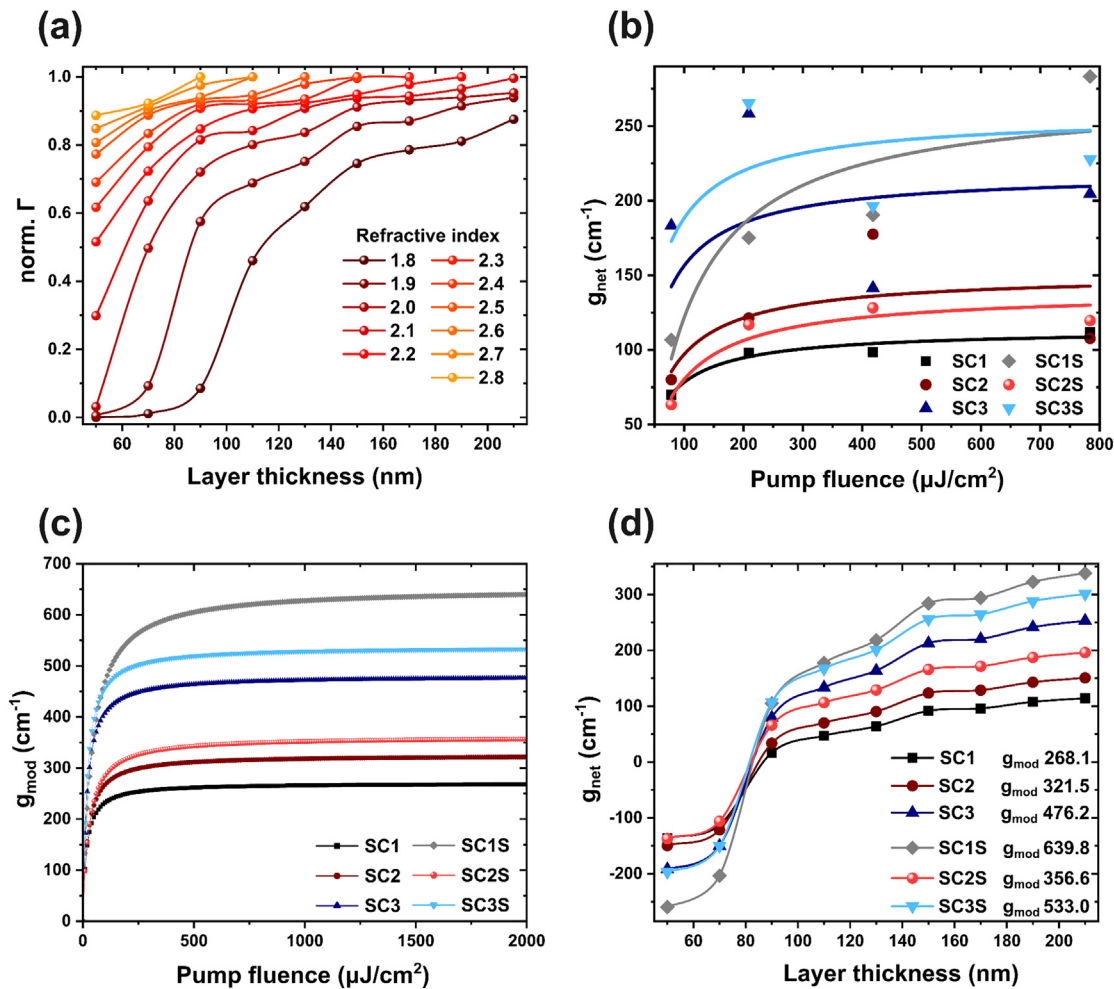


FIG. 3. (a) Thickness dependence of Γ for the films with different refractive indexes (see Table S4). (b) Measured net modal gain for different samples (dots). The numerical fit of the experimental data (solid line) by using Eq. (2). (c) Modal gain extracted from the fitting data for all the samples. (d) Calculated net modal gain values thickness dependence while maintaining α values of each sample.

For the samples SC2S and SC3S, the g_{mod} values increased in almost the same values and reached 356.6 and 533 cm⁻¹, respectively. Low SC2S g_{mod} values are due to stamping at a lower pressure of 1000 kg/cm². The magnitude of such changes depends on the relative increase in D of the film. In the samples with an initially high D , these changes are weaker.

The calculated n_t value of the sample characterizes a specific NPL film, taking into account the fluence level and efficiency of the optical pump applied to it. Thus, when evaluating g_{mat} of NPLs in the article by Foroutan-Barenji *et al.*, the calculated maximum value of the density of active centers of a 49 nm thick sample reached 459×10^{15} cm⁻³, which exceeds the value of 151×10^{15} cm⁻³ of the SC1S sample.¹⁸ This difference is determined by the advantage of the layer quality due to the self-assembly deposition at such a small thickness. The quantity of ideally packed $20 \times 20 \times 5$ nm³ NPLs is 500×10^{15} in 1 cm³, which coincides with the n_t obtained based on the corresponding material gain value. The NPL size of about $20 \times 20 \times 7$ nm³ used in this work gave 182×10^{15} NPLs in 1 cm³ and determined a packing

density of 0.829, which is comparable to or exceeds the highest values for the layers created by the spin-coating method and proves the advantages of the stamping process. Thus, the larger size of the platelets, while maintaining the internal structure, causes a decrease in the density of active centers, resulting in a decrease in optical gain.

To predict the optimal thickness of the light-emitting layer in the devices in terms of modal gain, g_{net} dependencies were constructed with the preservation of the α in the samples as well as the calculated Γ at $n = 1.9$ [Fig. 3(d)]. When the layer thickness exceeded 90 nm, the appearance of positive g_{net} values was noted. However, when the level of 200 nm was exceeded, the gain growth approached its saturation following the Γ values. It should be noted that with a change in the thickness and surface quality, the α values as well as F_s change, which will affect the shape of the curves describing real samples. However, based on the simulation results, it can be concluded that the highest g_{net} values can be obtained under the condition of the light-emitting layer thickness exceeding 200 nm. This conclusion coincides with the results of other reported studies, in which, for example, for a perovskite

CsPbBr₃ film, record values were obtained at a film thickness of 100–250 nm.¹⁹ A further increase in the thickness of the light-emitting layer will affect the pumping efficiency and, in electrically pumped devices, also the properties of charge carriers under the applied field.⁵

To summarize, we have shown that the modification by the flat stamping method improves the quality of the light-emitting layer, which is beneficial for lasing applications. Reducing the layer thickness has a negative effect on the g_{net} values; however, an increase in the density of active centers, n_r , allows us to completely overcome such an effect on a thickness range of 137.4–204.3 nm. Significant g_{mod} growth in all the samples when stamping with 1000 and 1500 kg/cm² was detected. Creation of polycrystalline film samples with a thickness of more than 200 nm and their subsequent stamping leads to obtaining the highest gain growth of both g_{net} , up to 1.26, and g_{mod} up to 2.39 times. In all samples, the g_{mod} values increased due to the growth of the n_r . Net modal gain analysis allows us to evaluate the properties of a specific sample and to model possible maximum values of the modal gain of such a material layer. It is also possible to evaluate the influence of the device design in terms of net modal gain.

The proposed method of film modification can be used as an additional step in the design of various light-emitting devices. The development of such devices opens opportunities across multiple fields, from general laser technologies to emerging areas of on-chip photonics,³² compact laser sources^{33,34} for high-performance computing,³⁵ and sensing.^{36,37}

See the [supplementary material](#) for NPL solution preparation, film deposition and flat stamping processes, morphological and optical properties of NPLs film, VSL optical measurements and the modal gain data fitting analysis, and Comsol Multiphysics numerical modeling results.

This work was supported by the National Natural Science Foundation of China (Project No. 62350610272). H.V.D. acknowledges support from the TUBA- Turkish Academy of Sciences and TUBITAK 2247-A National Leader Researchers Program (No. 121C266).

AUTHOR DECLARATIONS

Conflict of Interest

The authors have no conflicts to disclose.

Author Contributions

Ruslan Azizov: Conceptualization (equal); Data curation (lead); Formal analysis (lead); Investigation (lead); Visualization (lead); Writing – original draft (lead). **Jinlong Zhu:** Data curation (supporting); Investigation (supporting). **Pavel Talianov:** Investigation (supporting); Writing – review & editing (equal). **Hilmi Volkan Demir:** Supervision (equal); Writing – review & editing (equal). **Sergey Makarov:** Conceptualization (equal); Supervision (equal); Writing – review & editing (equal).

DATA AVAILABILITY

The data that support the findings of this study are available within the article and its [supplementary material](#).

REFERENCES

- N. Ahn, Y. S. Park, C. Livache, J. Du, K. Gungor, J. Kim, and V. I. Klimov, *Adv. Mater.* **35**(9), 2206613 (2023).
- W. B. Gunnarsson, K. Roh, L. Zhao, J. P. Murphy, A. J. Grede, N. C. Giebink, and B. P. Rand, *Chem. Rev.* **123**(12), 7548–7584 (2023).
- K. Tewari, D. Thapliyal, C. K. Bhargava, S. Verma, A. Mehra, S. Rana, and R. K. Arya, *Funct. Coat.: Innovations Challenges* **23**, 50 (2024).
- G. E. Cragg and A. L. Efros, *Nano Lett.* **10**(1), 313–317 (2010).
- J. Wu, L. Chen, Y. Zhao, Z. Xiong, W. Ji, and Y. Lei, *Appl. Phys. Lett.* **119**(7), 073303 (2021).
- N. Ahn, C. Livache, V. Pinchetti, and V. I. Klimov, *Chem. Rev.* **123**(13), 8251–8296 (2023).
- H. Jung, N. Ahn, and V. I. Klimov, *Nat. Photonics* **15**(9), 643–655 (2021).
- Y. S. Park, J. Roh, B. T. Diroll, R. D. Schaller, and V. I. Klimov, *Nat. Rev. Mater.* **6**(5), 382–401 (2021).
- A. Dey, J. Ye, A. De, E. Debroye, S. K. Ha, E. Bladt, and L. Polavarapu, *ACS Nano* **15**(7), 10775–10981 (2021).
- X. Liang, E. G. Durmusoglu, M. Lunina, P. L. Hernandez-Martinez, V. Valuckas, F. Yan, and H. V. Demir, *ACS Nano* **17**(20), 19981–19992 (2023).
- N. Ahn, C. Livache, V. Pinchetti, H. Jung, H. Jin, D. Hahm, and V. I. Klimov, *Nature* **617**(7959), 79–85 (2023).
- B. Guzelturk, Y. Kelestemur, M. Olutas, Q. Li, T. Lian, and H. V. Demir, *J. Phys. Chem. Lett.* **8**, 5317–5324 (2017).
- D. Dede, N. Taghipour, U. Quliyeva, M. Sak, Y. Kelestemur, K. Gungor, and H. V. Demir, *Chem. Mater.* **31**, 1818–1826 (2019).
- S. Delikanli, O. Erdem, F. Isik, H. D. Baruj, F. Shabani, H. B. Yagci, E. G. Durmusoglu, and H. V. Demir, *J. Phys. Chem. Lett.* **12**, 2177–2182 (2021).
- R. Duan, Z. Zhang, L. Xiao, X. Zhao, Y. T. Thung, L. Ding, Z. Liu, J. Yang, V. D. Ta, and H. Sun, *Adv. Mater.* **34**, 1–10 (2022).
- J. I. Climente, J. L. Movilla, and J. Planelles, *Small* **8**(5), 754–759 (2012).
- V. I. Klimov, *Annu. Rev. Condens. Matter Phys.* **5**(1), 285–316 (2014).
- S. Foroutan-Barenji, O. Erdem, N. Gheshlaghi, Y. Altintas, and H. V. Demir, *Small* **16**(45), 2004304 (2020).
- D. A. Tatarinov, S. S. Anoshkin, I. A. Tsibizov, V. Sheremet, F. Isik, A. Y. Zhizhchenko, and S. V. Makarov, *Adv. Opt. Mater.* **11**(7), 2202407 (2023).
- J. Q. Grim, S. Christodoulou, F. Di Stasio, R. Krahne, R. Cingolani, L. Manna, and I. Moreels, *Nat. Nanotechnol.* **9**, 891–895 (2014).
- C. She, I. Fedin, D. S. Dolzhnikov, P. D. Dahlberg, G. S. Engel, R. D. Schaller, and D. V. Talapin, *ACS Nano* **9**, 9475–9485 (2015).
- Z. Dikmen, A. T. Isik, I. Bozkaya, H. D. Baruj, B. Canimkurbey, F. Shabani, M. Ahmad, and H. V. Demir, *Nanoscale* **15**(22), 9745–9751 (2023).
- H. D. Baruj, I. Bozkaya, B. Canimkurbey, A. T. Isik, F. Shabani, S. Delikanli, and H. V. Demir, *Small* **19**(29), 2206582 (2023).
- B. Guzelturk, O. Erdem, M. Olutas, Y. Kelestemur, and H. V. Demir, *ACS Nano* **8**(12), 12524–12533 (2014).
- R. Azizov, I. Sinev, F. Isik, F. Shabani, A. Pushkarev, I. Yurdakul, H. V. Demir, and S. Makarov, *Appl. Phys. Lett.* **121**(22), 223301 (2022).
- K. L. Shaklee and R. F. Leheny, *Appl. Phys. Lett.* **18**(11), 475–477 (1971).
- B. Guzelturk, M. Pelton, M. Olutas, and H. V. Demir, *Nano Lett.* **19**, 277–282 (2019).
- M. Sharma, D. Savas, and H. V. Demir, *Proc. IEEE* **108**(5), 655–675 (2020).
- C. She, I. Fedin, D. S. Dolzhnikov, A. Demortiere, R. D. Schaller, M. Pelton, and D. V. Talapin, *Nano Lett.* **14**(5), 2772–2777 (2014).
- B. T. Diroll, B. Guzelturk, H. Po, C. Dabard, N. Fu, L. Makke, and S. Ithurria, *Chem. Rev.* **123**(7), 3543–3624 (2023).
- O. Aftenieva, M. Sudzius, A. Prudnikau, M. Adnan, S. Sarkar, V. Lesnyak, and T. A. König, *Adv. Opt. Mater.* **11**(6), 2202226 (2023).
- C. Grivas and M. Pollnau, *Laser Photonics Rev.* **6**, 419–462 (2012).
- F. Fan, O. Voznyy, R. P. Sabatini, K. T. Bicanic, M. M. Adachi, J. R. McBride, and E. H. Sargent, *Nature* **544**(7648), 75–79 (2017).
- O. V. Kozlov, Y. S. Park, J. Roh, I. Fedin, T. Nakotte, and V. I. Klimov, *Science* **365**(6454), 672–675 (2019).
- N. Savage, *IEEE Spectr.* **39**, 32–36 (2002).
- F. Vollmer and A. Stephen, *Nat. Methods* **5**(7), 591–596 (2008).
- A. Ziv, A. Tzaguy, Z. Sun, S. Yochelis, E. Stratakis, G. Kenanakis, G. C. Schatz, L. J. Lauhon, D. N. Seidman, Y. Paltiel, and R. Yerushalmi, *Nanoscale* **11**(13), 6368–6376 (2019).